Photothermal deflection in multilayer coatings: modeling and experiment

Laurent Gallais and Mireille Commandré

A model of the photothermal deflection signal in multilayer coatings is presented that takes into account optical interference effects and heat flow within the stack. Measurements are then taken of high-reflectivity HfO_2/SiO_2 ultraviolet mirrors made by plasma ion assisted deposition and compared to calculations. Good agreement is found between the experimental results and the model. Using this model for the calibration and the setup described, one can measure absorption in multilayer coatings accurately down to 10^{-7} of the incident power.

OCIS codes: 350.5340, 310.0310.

1. Introduction

The measurement of optical losses or thermal parameters in optical coatings is of great interest, for instance in the development of applications that use high-power systems. For this purpose, photothermal tools and in particular the photothermal deflection technique[1–6] are useful techniques for the characterization of absorption losses, with detectivity reaching 10^{-7} (Refs. 5 and 7), of the incident power and submicrometer resolution.[8] The measurement of single layer coatings with these techniques can be made quite easily if care is taken in the calibration. In the case of multilayer coatings, photothermal measurements are often used for the inspection of absorbing defects[9–11] (and possible connections with laser damage) to obtain the total absorption of the stack[12–14] or to separate the different contributions of substrate, film, volume, and interface absorption.[13–15] But, in such studies, interpretation or calibration is difficult because of the complex structure of the system (interference effects, absorption from the interface–layer volume, differences in thermal parameters, etc.). Then a theoretical approach must be associated with the measurements. In the case of multilayers, the calculation was made for the photoacoustic technique,[16] but, in the case of photothermal deflection (PD), although the theoretical approach in a monolayer has been described in detail in several papers,[1,5,17–19] no modeling of the photothermal signal has been done in a multilayer structure with optical interference effects and heat flow within the stack taken into account, though such a model could be of great interest for calibration of the signal, to dissociate the contributions of the layers and interfaces from the absorption and to extract thermal parameters from the measurements.

First we present the model that we developed. Then we apply it for various classic structures such as a mirror and a bandpass filter. Second, we present absorption measurements of a deep-ultraviolet mirror and calibrate them with our model. To finish, we discuss the limitations of the method and the advances and potential applications that can be obtained with this study.

2. Theory

A. Principles

The PD technique is based on the interaction of an intense modulated laser beam, called the pump beam, and the absorbing media. This interaction results in a temporal variation of temperature and then in a refractive-index gradient, surface bumping, and an acoustic wave, which are able to deflect a second laser beam, i.e., the probe beam. This deflection is measured and, by calibration, one can obtain the absorption value of the sample.

We have considered in our model the transmission configuration in which the pump and probe beams are normal to the surface and go through the sample

The authors are with the Institut Fresnel (Unité Mixte de Recherche, Centre National de la Recherche Scientifique), Ecole Généraliste d'Ingénieurs de Marseille, Aix Marseille I, Aix Marseille III, Domaine Universitaire de St Jérôme, 13397 Marseille Cedex 20, France. L. Gallais's e-mail address is laurent.gallais@fresnel.fr.

Received 8 December 2004; accepted 4 February 2005.
0003-6935/05/255230-09$15.00/0

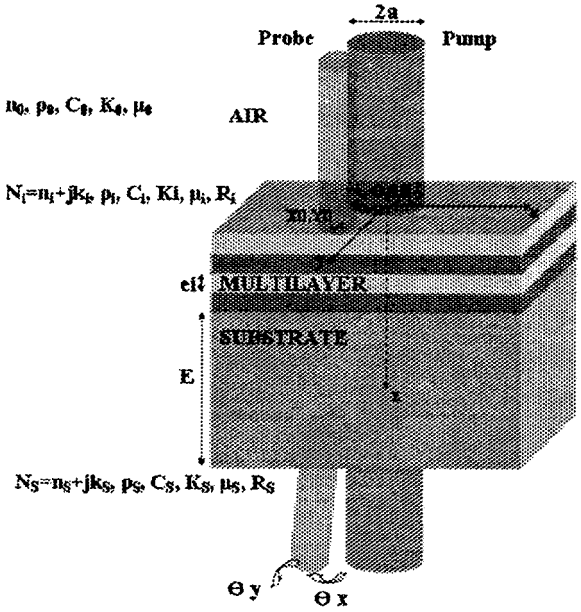

Fig. 1. Configuration and notation used in our model transmission calculation: n_i, k_i, real and imaginary parts of complex index N_i of medium i ($i = 0$ for air, $i = 1$ for the first layer, . . . , $i = N$ for the last layer, and $i = S$ for the substrate), K_i is the thermal conductivity, ρ_i is the mass density, C_i is the heat capacity per unit mass, R_i is the thermal resistance at the interface between media $i - 1$ and i, e_i is the film's thickness, and $2a$ is the diameter at $1/e^2$ of the Gaussian pump beam.

(Fig. 1). This configuration has been chosen for its great sensitivity and its ability to yield a high spatial resolution and to facilitate measurement in bulk material. The influence of the surface displacement on the sample is not considered: Indeed, previous studies of similar systems showed that the total deflection that is due to index gradients is greater than the deflection that is due to thermal expansion, in this configuration.[5] The probe beam is then deflected only by the radial index gradient in the air, the thin films, and the substrate.

The calculation of PD in these conditions is divided into two parts. First, by using the expression for the heat source that results from optical absorption in the thin films and in the substrate, we calculate the modulated temperature distribution in each medium: air, film, and substrate. Second, the effects of temperature distribution on the probe-beam propagation are calculated. Notice that in this calculation we have considered absorption only in bulk films, but interface absorption can also be modeled easily by the use of thin and absorbing layers at the interfaces.

B. Calculation of Modulated Temperature

We denote by $T_i(x, y, z, t)$ the time-dependent component of temperature distribution in medium i. The notation for the parameters is given in Fig. 1. The modeling was performed under some assumptions, as follows:

- The three media are isotropic and infinite in the x and y directions. The air and the substrate are also semi-infinite in the z direction.
- The pump and probe beams are parallel, are Gaussian in the x–y plane, and have a cylindrical symmetry in the z direction. Given that experimentally these two beams are Gaussian and focused on the surface of the sample, this hypothesis is valid only if the Rayleigh length of the pump beam is larger than the absorbing medium and the Rayleigh length of the probe beam is larger than the heated zone.
- The pump beam's waist is larger than the probe beam.
- Calculation is made under the assumption of unique heat conduction: Radiation losses and natural convection are negligible at ambient temperature.[20]

Given the cylindrical symmetry of the system, the temperature distribution keeps a cylindrical symmetry $T_i(r, z, t)$, where $r^2 = x^2 + y^2$, as for the pump beam. In this paper we are interested only in harmonic solutions: $T_i(r, z, t) = T_i(r, z)\exp(j\omega t)$, where $\omega = 2\pi F$ is the modulation pulsation of the pump beam.

Under these conditions, the temperature distribution in the various media satisfies the heat equations

$$\nabla^2 T_0(r, z, t) - \frac{\rho_0 C_0}{K_0}\frac{\partial T_0}{\partial t} = 0,$$

$$\nabla^2 T_i(r, z, t) - \frac{\rho_i C_i}{K_i}\frac{\partial T_i}{\partial t} = -\frac{Q_i(r, z, t)}{K_i},$$

$$\nabla^2 T_S(r, z, t) - \frac{\rho_S C_S}{K_S}\frac{\partial T_S}{\partial t} = -\frac{Q_S(r, z, t)}{K_S}, \qquad (1)$$

where $Q_i(r, z, t)$ are the heat sources that result from the optical absorption in medium i. They are calculated with the following equation, with interference and absorbing effects taken into account[5]:

$$Q_i(r, z, t) = \frac{4\pi k_i}{\lambda}\frac{n_i}{n_0}\frac{p_0}{\pi a^2}\exp\left(-\frac{2r^2}{a^2}\right) \times \exp(j\omega t)\left|\frac{E_i}{E_0^{+}}(z)\right|^2, \qquad (2)$$

where $E_i(z)$ is the electric field in medium i,

$$E_i(z) = E_i^{+}\exp\left(-j\frac{2\pi N_i}{\lambda}z\right) + E_i^{-}\exp\left(j\frac{2\pi N_i}{\lambda}z\right),$$

P_0 and E_0^{+} are, respectively, the incident power and field. The E_i values are calculated numerically through a classic thin-film calculation.[21]

To solve system (1) we use the radial Fourier transform of the temperature distribution and the following conditions (see Appendix A for details):

Continuity of temperature

$$T_0(r,\ z=0) = T_1(r,\ z=0) - \mathrm{Res}_0\ \Phi_{1\to A},$$

$$T_i(r,\ z=e_i) = T_{i+1}(r,\ z=e_i) - \mathrm{Res}_i\ \Phi_{i+1\to i},$$

$$T_N(r,\ z=e_N) = T_S(r,\ z=e_N) - \mathrm{Res}_N\ \Phi_{S\to N}, \qquad (3)$$

where Res_i is the interface resistivity.

Continuity of heat fluxes

$$\phi_{1\to A} = K_0 \left.\frac{\partial T_0}{\partial z}\right|_{z=0} = K_1 \left.\frac{\partial T_1}{\partial z}\right|_{z=0},$$

$$\phi_{i+1\to i} = K_i \left.\frac{\partial T_i}{\partial z}\right|_{z=ei} = K_{i+1} \left.\frac{\partial T_{i+1}}{\partial z}\right|_{z=ei},$$

$$\phi_{S\to N} = K_N \left.\frac{\partial T_N}{\partial z}\right|_{z=eN} = K_S \left.\frac{\partial T_S}{\partial z}\right|_{z=eN}, \qquad (4)$$

where $\phi_{i+1\to i}$ is the heat flux from layer $i+1$ to layer i.

After resolution of this system, the temperature distributions in the different media can be written as follows:

$$T_0(r,\ z,\ t) = 2\pi \int_0^{+\infty} \sigma J_0(2\pi\sigma r)\{A_0(\sigma) \times \exp[\alpha_0(\sigma)z]\}\mathrm{d}\sigma \exp(j\omega t),$$

$$\begin{aligned} T_i(r,\ z,\ t) = 2\pi \int_0^{+\infty} \sigma J_0(2\pi\sigma r)\Big\{ & A_i(\sigma)\exp[\alpha_i(\sigma)z] \\ & + B_i(\sigma)\exp[-\alpha i(\sigma)z] + F_i(\sigma)\Big[E_i^{+2} \\ & \times \exp\left(-\frac{4\pi k_i}{\lambda} z\right) + E_i^{-2} \exp\left(\frac{4\pi k_i}{\lambda} z\right)\Big] \\ & + G_i(\sigma)\Big[E_i^{+} E_i^{-*}\exp\left(-j\,\frac{4\pi n_i}{\lambda} z\right) \\ & + E_i^{+*} E_i^{-}\exp\left(j\,\frac{4\pi n_i}{\lambda} z\right)\Big]\Big\}\mathrm{d}\sigma \exp(j\omega t), \end{aligned}$$

$$\begin{aligned} T_s(r,\ z,\ t) = 2\pi \int_0^{+\infty} \sigma J_0(2\pi\sigma r)\Big\{ & B_S(\sigma) \\ & \times \exp[-\alpha_S(\sigma)(z)] + F_S(\sigma)E_S^{+2} \\ & \times \exp\left(-\frac{4\pi k_S}{\lambda} z\right)\Big\}\mathrm{d}\sigma \exp(j\omega t), \end{aligned} \qquad (5)$$

where A_i and B_i are calculated in Appendix A.

C. Photothermal Deflection

We neglect in the calculation the effect of the acoustic wave that accompanies the temperature rise. Given that and the conditions described above, the total shift of the probe beam in the x direction is small compared with the probe-beam diameter (x can be assumed constant along the beam path). The deflection in the x direction is given for medium i by

$$\theta_i = \frac{1}{n_i}\frac{\partial n_i}{\partial T}\int_{\text{path } i} \left[\frac{\partial T_i}{\partial x}(x,\ y,\ z,\ t)\right]_{x=x_0,\ y=y_0} \mathrm{d}z, \qquad (6)$$

where (x_0, y_0) is the shift between the centers of the pump and the probe beams in the plane $z = 0$.

Then, after derivation and integration, we find that

$$\begin{aligned} \theta_{y\ \mathrm{air}}(x_0,\ y_0,\ t) = & -\frac{1}{n_0}\frac{\partial n_0}{\partial T}\, 4\pi^2 \exp(j\omega t)\,\frac{y_0}{r_0}\int_0^{+\infty} \\ & \times \sigma^2 J_1(2\pi\sigma r_0)\,\frac{A_0}{\alpha_0}\,\mathrm{d}\sigma, \end{aligned}$$

$$\begin{aligned} \theta_{y\ \mathrm{couche}\ i}(x_0,\ y_0,\ t) = & -\frac{1}{n_i}\frac{\partial n_i}{\partial T}\, 4\pi^2 \exp(j\omega t)\,\frac{y_0}{r_0}\int_0^{+\infty} \\ & \times \sigma^2 J_1(2\pi\sigma r_0)\Bigg(\frac{A_i}{\alpha_i}\,[\exp(\alpha_i e_i) \\ & - \exp(\alpha_i e_{i-1})] + \frac{B_i}{\alpha_i}\,[\exp(-\alpha_i e_{i-1}) \\ & - \exp(-\alpha_i e_i)] + F_i\,\frac{\lambda}{4\pi k_i}\Big\{E_i^{+2} \\ & \times \left[\exp\left(-\frac{4\pi k_i}{\lambda}\,e_{i-1}\right) - \exp\right. \\ & \left.\times \left(-\frac{4\pi k_i}{\lambda}\,e_i\right)\right] + E_i^{-2}\left[\exp\left(\frac{4\pi k_i}{\lambda}\,e_i\right)\right. \\ & \left. - \exp\left(\frac{4\pi k_i}{\lambda}\,e_{i-1}\right)\right]\Big\} + G_i\,\frac{\lambda}{j4\pi n_i} \\ & \times \Big\{E_i^{+} E_i^{-*}\left[\exp\left(-\frac{j4\pi n_i}{\lambda}\,e_{i-1}\right)\right. \\ & \left. - \exp\left(-\frac{j4\pi n_i}{\lambda}\,e_i\right)\right] + E_i^{+*} E_i^{-} \\ & \times \left[\exp\left(\frac{j4\pi n_i}{\lambda}\,e_i\right)\right. \\ & \left. - \exp\left(\frac{j4\pi n_i}{\lambda}\,e_{i-1}\right)\right]\Big\}\Bigg)\mathrm{d}\sigma, \end{aligned}$$

$$\begin{aligned} \theta_{y\ \mathrm{substrate}}(x_0,\ y_0,\ t) = & \frac{1}{n_S}\frac{\partial n_S}{\partial T}\, 4\pi^2 \exp(j\omega t)\frac{y_0}{r_0}\int_0^{+\infty} \\ & \times \sigma^2 J_1(2\pi\sigma r_0)\Big\{\frac{B_S}{\alpha_S}\,[\exp(-\alpha_S e_N) \\ & - \exp(-\alpha_S E)] + F_S E_S^{+2}\,\frac{\lambda}{4\pi k_S} \\ & \times \left[\exp\left(-\frac{4\pi k_S}{\lambda}\,e_N\right)\right. \\ & \left. - \exp\left(-\frac{4\pi k_S}{\lambda}E\right)\right]\Big\}\mathrm{d}\sigma. \end{aligned} \qquad (7)$$

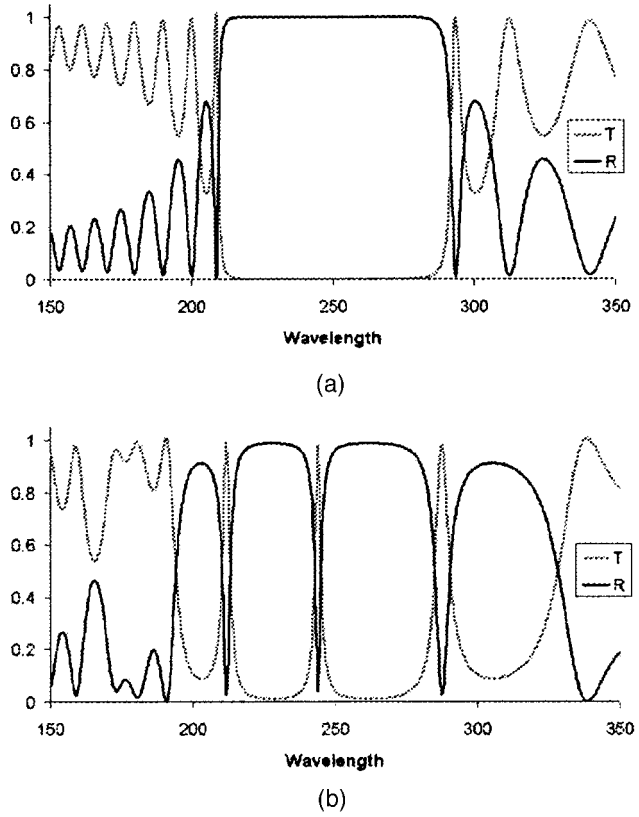

Fig. 2. Calculation of the spectral reflectance (R) and transmittance (T): (a) mirror M23, (b) Fabry–Perot filter: mirror M5, 12B, mirror M5. Materials: HfO_2 ($n = 2.4$) and SiO_2 ($n = 1.5$).

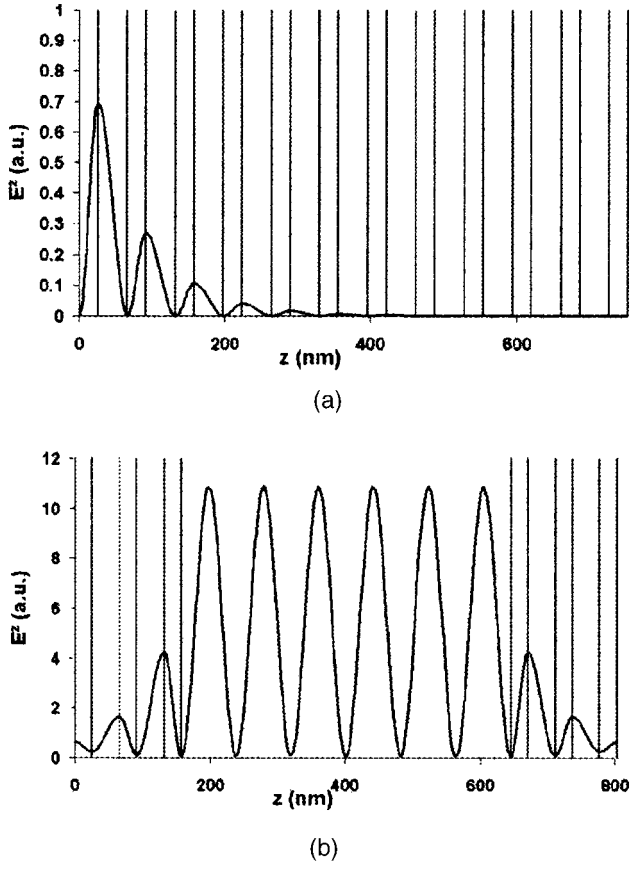

Fig. 3. Electric-field distribution calculated at 244 nm in (a) mirror M23, (b) Fabry–Perot filter: mirror M5, 12B, mirror M5. Materials: HfO_2 ($n = 2.4$) and SiO_2 ($n = 1.5$).

In the transmission configuration the total PD is the sum of the complex deflections in the three media: air, thin films, and substrate.

D. Applications

We present two examples of calculations with the model described above, applied for two thin-film optical components, a mirror M23 ($[HB]^{11}H$), and a Fabry–Perot filter, mirror M5–12B–mirror M5 ($[HB]^2H12B[HB]^2H$), centered at 244 nm (spectral reflectance and transmittance are calculated in Fig. 2), made from HfO_2 and SiO_2. For these materials we used in our computation the thermal parameters taken from Refs. 22–26. Note that there are few values in the literature for the thermal parameters of optical thin films, particularly for the thermo-optic coefficient. We did not find this value for HfO_2; consequently we used the same value as for SiO_2 in this calculation. The two systems (mirror and bandpass filter) have roughly the same optical thickness and are composed of the same materials, so only the electric-field distribution is changed (Fig. 3): It is localized near the surface for the mirror and enhanced in the spacer for the Fabry–Perot filter. We present in Fig. 4 our calculation of the relative PD versus shift distance between pump and probe beams for both systems, using the model presented above with an imaginary index of 10^{-4} (k) for the H and B layers. These calculations were made for a pump beam of 10 μm diameter at 244 nm and 1 kHz of modulation frequency.

We can observe that the two systems exhibit strongly different amplitude signals (ratio of almost 100) owing to differences in the electric-field distribution and subsequent absorption: Indeed, in the case of the Fabry–Perot filter the e-field enhancement in the spacer induced a strong absorption of optical power, whereas, in the mirror, absorption occurs only near the surface. In both cases the deflection is predominant in the stack (which has a total thickness of almost 800 nm) and consequently the thermal properties of the materials will have a great influence on the signal. This effect increases when the beam is focused or when the frequency increases.

3. Experiment

A. Experimental Setup

The experimental setup is shown in Fig. 5 (a detailed description is given in Ref. 27). It involves a 488 nm argon laser doubled at 244 nm with an external-cavity frequency doubler. The beam is modulated (1500 Hz in this study), spatially filtered, and focused onto the sample through one of a number of lenses, depending on the required pump-beam diameter. For

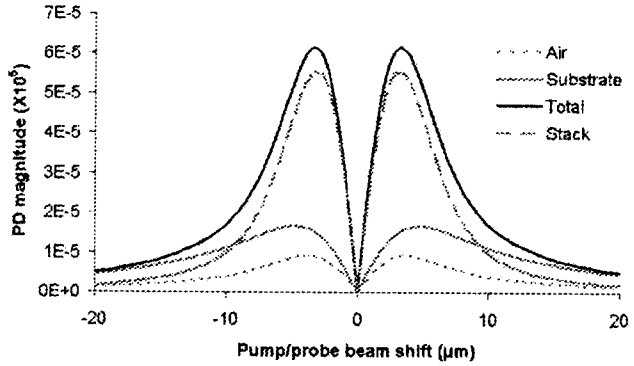

(a)

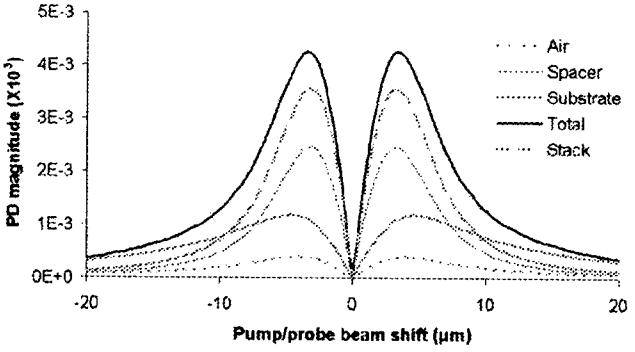

(b)

Fig. 4. Calculated photothermal deflection versus separation between pump and probe beams in (a), mirror M23, (b) Fabry–Perot filter: mirror M5, 12B, mirror M5. Materials: HfO_2 (K = 0.1 $Wm^{-1}K^{-1}$, ρC = 1.7 J $m^{-3}K^{-1}$, $\partial n/\partial T = 5E - 5K^{-1}$) and SiO_2 (K = 0.2 $W m^{-1}K^{-1}$, $\rho C = 1.5 \times 10^6$ J $m^{-3}K^{-1}$, $\partial n/\partial T = 5E - 5K^{-1}$).

this study the pump-beam waist was 30 μm and the probe-beam waist was 6 μm. The positions and sizes of the image waists of the pump and probe beams are checked with a knife-edge technique. In this configuration the Rayleigh length of the pump beam is larger than the absorbing medium (~1 μm for the multilayers under study). The Rayleigh length of the probe beam has to be larger than the heated zone to fulfill the conditions for the calculation (see Section 2). We calculated from Eqs. (5) the temperature

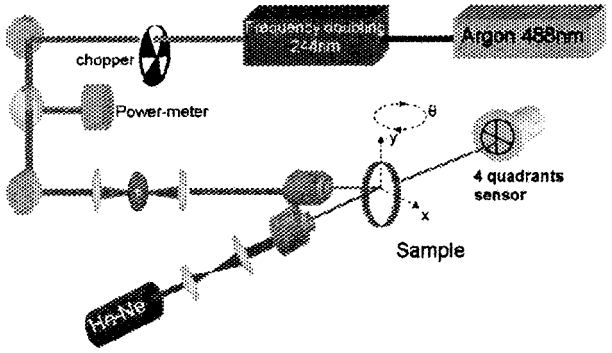

Fig. 5. Experimental setup for photothermal deflection measurements.

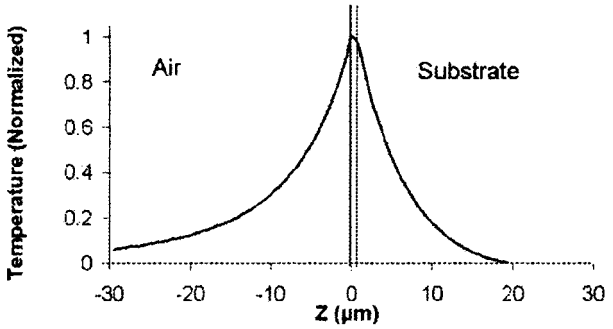

Fig. 6. Calculation of the temperature distribution in mirror M23 in our experimental configuration along the z axis at the center of the pump beam.

repartition in the sample under study (deep-ultraviolet mirror described below) and compared it to the Rayleigh length of the probe beam. The results, presented in Fig. 6, show that the condition that the probe beam's Rayleigh length (~350 μm) be larger than the heated zone is fulfilled.

The deflection of the probe beam is measured in this setup with a quadrant sensor. The lowest absorption that we can detect with this apparatus is related to the background noise in the case of a nonabsorbing sample: The noise equivalent absorptance equals 0.4 parts in 10^6 with 200 mW pump power.[28]

B. Study of a Deep-Ultraviolet Mirror

We used the model presented above to analyze and interpret measurements in a practical case: that of a high-reflectivity HfO_2/SiO_2 ultraviolet mirror $([HB]^{11}H)$ centered at 250 nm, made at the Institut Fresnel by plasma ion assisted deposition (more details on the method of manufacture can be found in Ref. 29). For this sample the various optical and thermal parameters that were used in the calculation are summarized in Tables 1 and 2. These parameters were either measured in the laboratory or found in the literature.

For this sample we measured the PD signal to obtain its absorption. First the signal (amplitude and phase) was measured as a function of the pump–probe-beam shift and compared with calculations (Fig. 7). Good agreement was obtained, and the model is a good description of the photothermal signal.

Then, to obtain the absorption from this measurement, we performed the appropriate calibration procedure. Indeed, the absorption measurement is indirect, and the PD signal (PDS) is strongly dependent on the thermal parameters of the sample under study. The PDS is related to the absorption of the sample (A_{Sample}): $A_{\text{Sample}} = \alpha \times \beta_{\text{sample}} \times \text{PDS}_{\text{sample}}$, where β_{sample} is a constant that depends on the sample's properties and α is a constant that depends on experimental conditions. The calibration procedure that we used is based on a comparison of the signal of sample $\text{PDS}_{\text{sample}}$ with a calibration sample (CS) of well-known absorption. We have

Table 1. Optical Parameters of the HfO_2 Layers

Parameter	n	k	e (nm)	K (W m^{-1} s^{-1})	ρC (J m^{-3} K^{-1})	$\partial n/\partial T$ (K^{-1})
Value	2.25[a]	0.0025[a]	28 nm[a]	1.7[b]	1.71×10^6 (bulk)	Unknown

[a]Ref. 29.
[b]Refs. 24 and 25.

Table 2. Optical Parameters of the SiO_2 Layers

Parameter	n	k	e (nm)	K (W m^{-1} s^{-1})	ρC (J m^{-3} K^{-1})	$\partial n/\partial T$ (K^{-1})
Value	1.52[a]	0.0015[a]	41 nm[a]	1[b]	1.46×10^6 (bulk)	5×10^{-5}[c]

[a]Ref. 29.
[b]Ref. 25.
[c]Ref. 26.

$$A_{\mathrm{CS}} = \alpha \times \beta_{\mathrm{CS}} \times \mathrm{PDS}_{\mathrm{CS}}, \tag{8}$$

$$A_{\mathrm{sample}} = \alpha \times \beta_S \times \mathrm{PDS}_{\mathrm{Sample}}. \tag{9}$$

The absorption of the sample can be deduced as follows:

$$A_{\mathrm{sample}} = A_{\mathrm{CS}} \frac{\beta_S \mathrm{PDS}_{\mathrm{sample}}}{\beta_{\mathrm{CS}} \mathrm{PDS}_{\mathrm{CS}}}. \tag{10}$$

A_{CS} is known, the PDSs are measured, and β are calculated with our model.

The calibrated absorbing samples were obtained by implantation of titanium into fused-silica substrates and measured with a spectrophotometer (more details can be found in Refs. 28 and 30). By adjusting the ion dose we obtained four calibrated absorbing samples, to which we refer as samples 1, 2, 3, and 4 ($A_1 = 0.48$, $A_2 = 0.15$, $A_3 = 0.02$, and $A_4 = 0.006$). The photothermal deflection signal was measured on the mirror and on the various calibrated samples. The results are illustrated in Fig. 8.

Then, by applying the calibration procedure described above, we obtained the absorption of the mirror. We found that 0.005 ± 0.002. The uncertainty in this measurement is due to the fact that the HfO_2 thermo-optic coefficient is unknown (it varied from -10^{-4} to 10^{-4} in the calculation of β).

The theoretical absorption of the mirror can be calculated because we know the extinction coefficients of these two materials (see Tables 1 and 2):

$$A_{\mathrm{stack}} = \sum_i \frac{4\pi k_i}{\lambda} \frac{n_i}{n_0} \int_{e_{i-1}}^{e_i} \left| \frac{E_i}{E_0^+}(z) \right|^2 \mathrm{d}z. \tag{11}$$

We found a theoretical absorption of 0.009, which is similar to the calculated value. The little difference can be explained by uncertainties that have not been taken into account in our measurement and calibration procedure (mostly uncertainties in the thermal conductivity value of both materials, and in the alignment of the two beams) but also by uncertainties in the extinction index measurements.

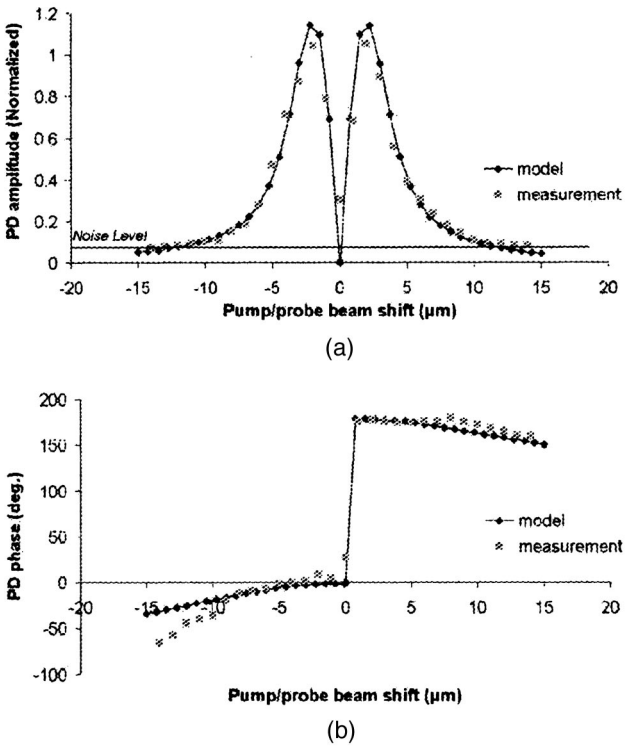

Fig. 7. Measurement and theoretical PD versus separation between pump and probe beams in mirror M23: (a) amplitude; (b) phase.

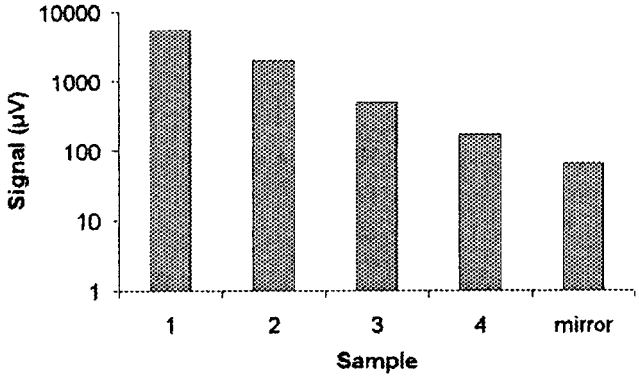

Fig. 8. Measurement of the photothermal signal on the calibration samples and on the deep-ultraviolet mirror.

4. Discussion

The main difficulty in using the PD technique to measure losses in multilayer components is in the calibration of the absorption. Without this calibration, if one assumes a simple proportionality between the PDS of a calibration sample and the unknown sample, the error can be quite significant. The model presented above permits a rigorous measurement of the absorption, but it requires a good knowledge of the sample properties. The problem is that for thin-film materials we lack accurate numerical values for their thermal properties (mainly for $\partial n/\partial T$). To get around this problem, solutions can be the use of a large beam or a low frequency or both for the measurement: Then the deflection is no longer predominant in the multilayer, and the error is minimized. But in this case we do not have access to measurement of local absorption. However, when the PDS is strongly dependent on the material properties a detailed study of the signal's (amplitude and phase) dependence on experimental parameters (frequency, beam size, pump–probe beam shift, wavelength, incidence, etc.) can give access to values of these properties by fits of the measurements with the model.

5. Conclusions

A calculation of the photothermal deflection signal in multilayer coatings was presented. The model has been applied to the study of the deflection signal in different systems (mirror, bandpass filter) and to the interpretation of absorption measurement of a high-reflectivity HfO_2/SiO_2 deep-ultraviolet mirror. Good agreement has been obtained between measurements and theoretical values.

Using the system and the model presented in this paper, one may measure accurately absolute absorption in multilayer coatings down to 10^{-7} of the incident power. Other applications could be the determination of thermal properties and discrimination between interface and volume absorption of complex systems such as multilayer coatings.

Appendix A: Calculation of the Temperature Distribution

$T_i(r, z)$ is the solution of the system

$$\nabla^2 T_0(r,\ z,\ t) - \frac{\rho_0 C_0}{K_0}\frac{\partial T_0}{\partial t} = 0,$$

$$\nabla^2 T_i(r,\ z,\ t) - \frac{\rho_i C_i}{K_i}\frac{\partial T_i}{\partial t} = -\frac{2R_i}{\pi a^2}\exp\left(-\frac{2r^2}{a^2}\right) \times \exp(j\omega t)\left|\frac{E_i}{E_0^{+}}(z)\right|^2,$$

$$\nabla^2 T_S(r,\ z,\ t) - \frac{\rho_2 C_2}{K_S}\frac{\partial T_S}{\partial t} = -\frac{2R_S}{\pi a^2}\exp(j\omega t)\left|\frac{E_S}{E_0^{+}}(z)\right|^2, \quad \text{(A1)}$$

with

$$R_i = \frac{P_0}{2K_i}\frac{n_i}{n_0}\frac{4\pi k_i}{\lambda}.$$

We consider the radial Fourier transform

$$T_i(r,\ z) = 2\pi\int_0^{+\infty}\sigma J_0(2\pi\sigma r)\tilde{T}_i(\sigma,\ z)\mathrm{d}\sigma, \quad \text{(A2)}$$

where $\tilde{T}_i(\sigma, z)$ is the radial Fourier transform of the temperature. Then system (A1) becomes

$$\frac{\partial^2}{\partial z^2}\tilde{T}_0(\sigma,\ z,\ t) - {\alpha_0}^2(\sigma)\tilde{T}_0(\sigma,\ z,\ t) = 0,$$

$$\frac{\partial^2}{\partial z^2}\tilde{T}_i(\sigma,\ z,\ t) - {\alpha_i}^2(\sigma)\tilde{T}_i(\sigma,\ z,\ t) = -R_i \times \exp\left(-\frac{a^2\sigma^2\pi^2}{2}\right)\exp(j\omega t)\left|\frac{E_i}{E_0^{+}}(z)\right|^2,$$

$$\frac{\partial^2}{\partial z^2}\tilde{T}_S(\sigma,\ z,\ t) - {\alpha_S}^2(\sigma)\tilde{T}_S(\sigma,\ z,\ t) = -R_S \times \exp\left(-\frac{a^2\sigma^2\pi^2}{2}\right)\exp(j\omega t)\left|\frac{E_S^{+}}{E_0^{+}}\right|^2\exp\left(-\frac{4\pi k_S}{\lambda}z\right), \quad \text{(A3)}$$

with

$$\mu_i = \left(\frac{K_i}{\rho_i C_i \pi F}\right)^{1/2}, \qquad {\alpha_i}^2 = 4\pi^2\sigma^2 + \frac{2j}{{\mu_i}^2},$$

$$R_i = \frac{P_0}{2K_i}\frac{n_i}{n_0}\frac{4\pi k_i}{\lambda}.$$

Using the limit conditions, we obtain for the transform of the temperature

$$\tilde{T}_0(\sigma,\ z,\ t) = A_0(\sigma)\exp[\alpha_0(\sigma)z]\exp(j\omega t),$$

$$\tilde{T}_i(\sigma,\ z,\ t) = \Big\{A_i(\sigma)\exp[\alpha_i(\sigma)z] + \beta_i(\sigma)\exp[-\alpha_i(\sigma)z] + F_i(\sigma)\Big[{E_i}^{+2}\exp\left(-\frac{4\pi k_i}{\lambda}z\right) + {E_i}^{-2}\exp\left(\frac{4\pi k_i}{\lambda}z\right)\Big] + G_i(\sigma)\Big[E_i^{+}{E_i}^{-*} \times \exp\left(-j\frac{4\pi n_i}{\lambda}z\right) + {E_i}^{+*}{E_i}^{-}\exp\left(j\frac{4\pi n_i}{\lambda}z\right)\Big]\Big\}\exp(j\omega t),$$

$$\tilde{T}_S(\sigma,\ z,\ t) = \Big\{B_S(\sigma)\exp[-\alpha_2(\sigma)z] + F_S(\sigma){E_S}^{+2} \times \exp\left(-\frac{4\pi k_S}{\lambda}z\right)\Big\}\exp(j\omega t), \quad \text{(A4)}$$

with

$$F_i(\sigma) = \frac{1}{\left|E_0^{+2}\right|} \frac{R_i \exp(a^2\sigma^2\pi^2/2)}{\alpha_i{}^2(\sigma) - (4\pi k_i/\lambda)^2},$$

$$G_i(\sigma) = \frac{1}{\left|E_0^{+2}\right|} \frac{B_i \exp[-(a^2\sigma^2\pi^2/2)]}{\alpha_i{}^2(\sigma) + (4\pi n_i/\lambda)^2}.$$

Given boundary conditions (3), $A_i(\sigma)$ and $B_i(\sigma)$ are solutions of the system

$$\begin{aligned} T_i(r,\, z,\, t) = 2\pi \int_0^{+\infty} \sigma J_0(2\pi\sigma r) \Big\{ & A_i(\sigma)\, \exp[\alpha_i(\sigma) z] \\ & + B_i(\sigma)\, \exp[-\alpha_i(\sigma) z] + F_i(\sigma) \\ & \times \left[E_i^{+2} \exp\left(\frac{4\pi k_i}{\lambda} z\right) + E_i^{-2} \exp\left(\frac{4\pi k_i}{\lambda} z\right) \right] \\ & + G_i(\sigma) \left[E_i^{+} E_i^{-*} \exp\left(-j\frac{4\pi n_i}{\lambda} z\right) \right. \\ & \left. + E_i^{+*} E_i^{-} \exp\left(j\frac{4\pi n_i}{\lambda} z\right) \right] \Big\} \mathrm{d}\sigma\, \exp(\mathrm{j}\omega t), \end{aligned}$$

$$\begin{bmatrix} & (1+h_0) & -1 & -1 & \dots \\ & K_0\alpha_0 & -K_1\alpha_1 & K_1\alpha_1 & \dots \\ \dots & \dots & \dots & \dots & \dots \\ & (1+h_i)\exp(-\alpha_i e_i) & (1-h_i)\exp(-\alpha_i e_i) & -\exp(\alpha_{i+1} e_i) & -\exp(-\alpha_{i+1} e_i) \\ & K_i\alpha_i\ \exp(\alpha_i e_i) & -K_i\alpha_i\ \exp(-\alpha_i e_i) & -K_{i+1}\alpha_{i+1}\ \exp(\alpha_{i+1} e_i) & K_{i+1}\alpha_{i+1}\ \exp(-\alpha_{i+1} e_i) \\ \dots & \dots & \dots & \dots & \dots \\ \dots & & (1+h_N)\exp(\alpha_N e_N) & (1-h_N)\exp(-\alpha_N e_N) & -\exp(-\alpha_S e_N) \\ \dots & & K_N\alpha_N\ \exp(\alpha_N e_N) & -K_N\alpha_N\ \exp(-\alpha_N e_N) & K_S\alpha_S\ \exp(-\alpha_S e_N) \end{bmatrix} \begin{pmatrix} A_0 \\ A_1 \\ B_1 \\ \vdots \\ A_i \\ B_i \\ A_{i+1} \\ B_{i+1} \\ \vdots \\ A_N \\ B_N \\ B_S \end{pmatrix} \tag{A5}$$

$$= \begin{bmatrix} F_1 a_1(0) + G_1 b_1(0) \\ g_1 F_1 a_1{}'(0) + j f_1 G_1 b_1{}'(0) \\ \dots \\ -F_i a_i(e_i) - G_i b_i(e_i) + F_{i+1} a_{i+1}(e_i) + G_{i+1} b_{i+1}(e_i) - \mathrm{Res}_i\, g_i F_i a_i{}'(e_i) - j\, \mathrm{Res}_i\, f_i G_i b_i{}'(e_i) \\ -g_i F_i a_i{}'(e_i) - j f_i G_i b_i{}'(e_i) + g_{i+1} F_{i+1} a_{i+1}{}'(e_i) + j f_{i+1} G_{i+1} b_{i+1}{}'(e_i) \\ \dots \\ -F_N a_N(e_N) - G_N b_N(e_N) + F_S a_S(e_N) - g_N\, \mathrm{Res}_N\, F_N a_N{}'(e_N) - j\, \mathrm{Res}_N\, f_N G_N b_N{}'(e_N) \\ -g_N F_N a_N{}'(e_N) - j f_N G_N b_N{}'(e_N) + g_S F_S a_S{}'(e_N) \end{bmatrix} \tag{A6}$$

with $h_i(\sigma) = \mathrm{Res}_i\, K_i\alpha_i$, $g_i = K_i(4\pi k_i/\lambda)$, $f_i = K_i(4\pi n_i/\lambda)$, $a_i(e_j) = E_i^{+2} \exp[-(4\pi k_i/\lambda)e_j] + E_i^{-2} \exp[(4\pi k_i/\lambda)e_j]$, $b_i(e_j) = E_i^{+} E_i^{-*} \exp[-j(4\pi n_i/\lambda)e_j] + E_i^{+*} E_i^{-} \exp[j(4\pi n_i/\lambda)e_j]$, $a_i{}'(e_j) = -E_i^{+2} \exp[(4\pi k_i/\lambda)e_j] + E_i^{-2} \exp[(4\pi k_i/\lambda)e_j]$, $b_i{}'(e_j) = -E_i^{+} E_i^{-*} \exp[-j(4\pi n_i/\lambda)e_j] + E_i^{+*} E_i^{-} \exp[j(4\pi n_i/\lambda)e_j]$.

After a numerical resolution of this system, the temperature distributions in the three media can be written as follows:

$$\begin{aligned} T_0(r,\, z,\, t) = 2\pi \int_0^{+\infty} & \sigma J_0(2\pi\sigma r) \{ A_0(\sigma) \\ & \times \exp[\alpha_0(\sigma) z] \} \mathrm{d}\sigma\, \exp(j\omega t), \end{aligned}$$

$$\begin{aligned} T_S(r,\, z,\, t) = 2\pi \int_0^{+\infty} & \sigma J_0(2\pi\sigma r) \Big\{ B_S(\sigma) \exp[-\alpha_2(\sigma)(z)] \\ & + F_S(\sigma) E_S^{+2} \exp\left(-\frac{4\pi k_S}{\lambda} z\right) \Big\} \mathrm{d}\sigma\, \exp(j\omega t). \end{aligned} \tag{A7}$$

The authors are grateful to P. Torchio of the Institut Fresnel for furnishing the samples.

References

1. A. C. Boccara, D. Fournier, W. Jackson, and N. M. Amer, "Sensitive photothermal deflection technique for measuring absorption in optically thin media," Opt. Lett. **5,** 377–379 (1980).

2. J. C. Murphy and L. C. Aamodt, "Photothermal spectroscopy using optical beam probing: mirage effect," J. Appl. Phys. **51,** 4580–4588 (1980).
3. E. Welsh and D. Ristau, "Photothermal measurements on optical thin films," Appl. Opt. **34,** 7339–7253 (1995).
4. M. Commandré and E. Pelletier, "Measurement of absorption losses in TiO_2 films by a collinear photothermal deflection technique," Appl. Opt. **29,** 4276–4283 (1990).
5. M. Commandré and P. Roche, "Characterization of optical coatings by photothermal deflection," Appl. Opt. **35,** 5021–5034 (1996).
6. Z. Wu, M. Thomsen, P. Kuo, Y. Lu, C. Stolz, and M. Koslowski, "Photothermal characterization of optical thin film coatings," Opt. Eng. **36,** 251–262 (1997).
7. V. Loriette and C. Boccara, "Absorption of low-loss optical materials measured at 1064 nm by a position-modulated collinear photothermal detection technique," Appl. Opt. **42,** 649–656 (2003).
8. A. During, C. Fossati, and M. Commandré, "Photothermal deflection microscopy for imaging submicronic defects in optical materials," Opt. Commun. **230,** 279–286 (2004).
9. W. Mundy, J. Ermshar, P. Hanson, and R. Hughes, "Photothermal deflection microscopy of HR and AR coatings," in *Laser-Induced Damage in Optical Materials: 1983*, H. E. Bennett, A. H. Guenther, D. Milam, and B. E. Newman, eds., Nat. Bur. Stand. (U.S.) Spec. Publ. **688,** 360–371 (1983).
10. A. Papandrew, C. Stolz, Z. Wu, G. Loomis, and S. Falabella, "Laser conditioning characterization and damage threshold prediction of hafnia/silica multilayer mirrors by photothermal microscopy," in *Laser-Induced Damage in Optical Materials: 2000*, G. J. Exarhos, A. H. Guenther, M. R. Kozlowski, K. L. Lewis, and M. J. Soileau, eds., Proc. SPIE **4347,** 53–61 (2001).
11. A. During, M. Commandré, C. Fossati, B. Bertussi, J. Y. Natoli, J. L. Rullier, H. Bercegol, and P. Bouchut, "Integrated photothermal microscope and laser damage test facility for *in-situ* investigation of nanodefect induced damage," Opt. Express **11,** 2497–2501 (2003).
12. D. Ristau, X. Dang, and J. Ebert, "Interface and bulk absorption of oxide layers and correlation to damage threshold," in *Laser-Induced Damage in Optical Materials: 1985,* H. E. Bennett, A. H. Guenther, D. Milam, and B. E. Newman, eds., Natl. Bur. Stand. (U.S.) Spec. Publ. **727,** 298–312 (1986).
13. E. Welsh, H. Walther, R. Wolf, D. Schafer, and L. Wieczorek, "Measurement of optical losses and damage threshold of multilayer coatings," Thin Solid Films **117,** 87–94 (1984).
14. E. Welsh, H. Walther, D. Schafer, and R. Wolf, "Measurement of optical losses and damage resistance of ZnS–Na_3AlF_6 and TiO_2–SiO_2 laser mirrors depending on coating design," Thin Solid Films **152,** 433–442 (1987).
15. E. Welsh, H. Walther, D. Schafer, R. Wolf, and H. Muller, "Correlation between morphology, optical losses and laser damage of MgF_2–SiO_2 multilayers," Thin Solid Films **156,** 1–10 (1988).
16. H. Walther, E. Welsh, and J. Opfermann, "Calculation and measurement of the absorption in multilayer films by means of photoacoustics," Thin Solid Films **142,** 27–35 (1986).
17. W. Jackson, N. M. Amer, A. C. Boccara, and D. Fournier, "Photothermal deflection spectroscopy and detection," Appl. Opt. **20,** 1333–1344 (1981).
18. M. A. Olmstead, N. M. Amer, S. Kohn, D. Fournier, and A. C. Boccara, "Photothermal displacement spectroscopy: an optical probe for solids and surfaces," Appl. Phys. **32,** 141–154 (1983).
19. P. Zimmermann and E. Welsch, "Modeling of signal detection by using the photothermal probe beam deflection technique," Rev. Sci. Instrum. **65,** 97–101 (1994).
20. G. Rousset, F. Charbonnier, and F. Lepoutre, "Influence of radiative and convective transfers in a photothermal experiment," J. Appl. Phys. **56,** 2093–2096 (1984).
21. H. A. Macleod, *Thin-Film Optical Filters* (Adam Hilger, 1986).
22. D. Decker, L. Koshigoe, and E. Ashley, "Thermal properties of optical thin film materials," in *Laser-Induced Damage in Optical Materials: 1984,* H. E. Bennett, A. H. Guenther, D. Milam, and B. E. Newman, eds., Natl. Bur. Stand. (U.S.) Spec. Publ. **727,** 291–297 (1986).
23. D. Ristau and J. Ebert, "Development of a thermographic laser calorimeter," Appl. Opt. **25,** 4571–4578 (1986).
24. J. Lambropoulos, M. Jolly, C. Amsden, S. Gilman, M. Sinicropi, D. Diakomihalis, and S. Jacobs, "Thermal conductivity of dielectric thin films," J. Appl. Phys. **66,** 4230–4242 (1989).
25. S. Lee, D. Cahill, and T. Allen, "Thermal conductivity of sputtered oxide films," Phys. Rev. B **52,** 253–257 (1995).
26. E. Drouard, P. Huguet-Chantõme, L. Escoubas, and F. Flory, "$\partial n/\partial T$ measurements performed with guided waves and their application to the temperature sensitivity of wavelength-division multiplexing filters," Appl. Opt. **41,** 3192–3136 (2002).
27. L. Gallais, H. Hinsch, M.-L. Lay, and M. Commandré, "Photothermal facility for optical characterization of DUV materials," in *Advances in Optical Thin Films,* C. Amra, N. Kaiser, and H. Angus Macleod, eds. Proc. SPIE **5250,** 597–602 (2004).
28. L. Gallais and M. Commandré, "Simultaneous absorption, scattering, and luminescence mappings for the characterization of optical coatings and surfaces," Appl. Opt. (to be published).mc
29. P. Torchio, A. Gatto, M. Alvisi, G. Albrand, N. Kaiser, and C. Amra, "High-reflectivity HfO_2/SiO_2 ultraviolet mirrors," Appl. Opt. **41,** 3156–3261 (2002).
30. S. Tisserand, F. Flory, A. Gatto, L. Roux, M. Adamik, and I. Kovacs, "Titanium implantation in bulk and thin film amorphous silica," J. Appl. Phys. **83,** 5150–5153 (1998).